Draft version March 23, 2012
Preprint typeset using LaTeX style emulateapj v. 5/2/11

arXiv:1203.4839v1 [astro-ph.SR] 21 Mar 2012

CONSTRAINING TYPE Ia SUPERNOVA MODELS: SN 2011fe AS A TEST CASE

F. K. Röpke,[1,2] M. Kromer,[2] I. R. Seitenzahl,[1,2] R. Pakmor,[3] S. A. Sim,[4] S. Taubenberger,[2] F. Ciaraldi-Schoolmann,[2] W. Hillebrandt,[2] G. Aldering,[5] P. Antilogus,[6] C. Baltay,[7] S. Benitez-Herrera,[2] S. Bongard,[6] C. Buton,[8] A. Canto,[6] F. Cellier-Holzem,[6] M. Childress,[5,9] N. Chotard,[10] Y. Copin,[10] H. K. Fakhouri,[5,9] M. Fink,[1,2] D. Fouchez,[13] E. Gangler,[10] J. Guy,[6] S. Hachinger,[2] E. Y. Hsiao,[5] C. Juncheng,[14] M. Kerschhaggl,[8] M. Kowalski,[8] P. Nugent,[11] K. Paech,[8] R. Pain,[6] E. Pecontal,[12] R. Pereira,[10] S. Perlmutter,[5,9] D. Rabinowitz,[7] M. Rigault,[10] K. Runge,[5] C. Saunders,[5,9] G. Smadja,[10] N. Suzuki,[5] C. Tao,[13,14] R. C. Thomas,[11] A. Tilquin,[13] C. Wu[6,15]

Draft version March 23, 2012

ABSTRACT

The nearby supernova SN 2011fe can be observed in unprecedented detail. Therefore, it is an important test case for Type Ia supernova (SN Ia) models, which may bring us closer to understanding the physical nature of these objects. Here, we explore how available and expected future observations of SN 2011fe can be used to constrain SN Ia explosion scenarios. We base our discussion on three-dimensional simulations of a delayed detonation in a Chandrasekhar-mass white dwarf and of a violent merger of two white dwarfs—realizations of explosion models appropriate for two of the most widely-discussed progenitor channels that may give rise to SNe Ia. Although both models have their shortcomings in reproducing details of the early and near-maximum spectra of SN 2011fe obtained by the Nearby Supernova Factory (SNfactory), the overall match with the observations is reasonable. The level of agreement is slightly better for the merger, in particular around maximum, but a clear preference for one model over the other is still not justified. Observations at late epochs, however, hold promise for discriminating the explosion scenarios in a straightforward way, as a nucleosynthesis effect leads to differences in the ^{55}Co production. SN 2011fe is close enough to be followed sufficiently long to study this effect.

Subject headings: Supernovae: general—supernovae: individual (SN 2011fe)—hydrodynamics—nuclear reactions, nucleosynthesis, abundances

1. INTRODUCTION

Perhaps the most fundamental problem hindering a better understanding of SN Ia explosions is the unclear nature of the progenitor system. One way of addressing this problem is to carry out numerical simulations for different scenarios that involve thermonuclear explosions of white dwarfs (WDs) and to compare the results with observations. Obviously, detailed observational data are a prerequisite for this approach. At the same time, the comparison should be based on models that avoid free parameters in the description of the explosion mechanism, as far as possible. Only then the predictive power of theoretical models will be sufficient to discriminate between explosion models and to draw conclusions about progenitor systems.

In addition to the possibility of directly constraining the progenitor system from archival data (Li et al. 2011; Liu et al. 2011) or early observations (Brown et al. 2011; Nugent et al. 2011b; Bloom et al. 2012), the recently discovered nearby SN Ia 2011fe offers a unique opportunity for a comparison with explosion models. Of particular value are the possibility to follow this close object photometrically to extremely late epochs and the exact knowledge of the explosion time.

SN 2011fe was first detected by the Palomar Transient Factory on 2011 August 24.167 in M101 (Nugent et al. 2011a). A preliminary analysis of our data indicates that it reached an apparent B-band peak magnitude of 9.9 on September 11. Combined with the derived explosion date of 2011 August 23.7 (Nugent et al. 2011b), the B-band rise time of SN 2011fe is $\sim$18.3 d—a typical value for normal SNe Ia (Conley et al. 2006;

[1] Institut für Theoretische Physik und Astrophysik, Universität Würzburg, Am Hubland, D-97074 Würzburg, Germany
[2] Max-Planck-Institut für Astrophysik, Karl-Schwarzschild-Str. 1, D-85741 Garching, Germany
[3] Heidelberger Institut für Theoretische Studien, Schloss-Wolfsbrunnenweg 35, 69118 Heidelberg, Germany
[4] Research School of Astronomy and Astrophysics, The Australian National University, Mount Stromlo Observatory, Cotter Road, Weston Creek ACT 2611 Australia
[5] Physics Division, Lawrence Berkeley National Laboratory, 1 Cyclotron Road, Berkeley, CA, 94720
[6] Laboratoire de Physique Nucléaire et des Hautes Énergies, Université Pierre et Marie Curie Paris 6, Université Paris Diderot Paris 7, CNRS-IN2P3, 4 place Jussieu, 75252 Paris Cedex 05, France
[7] Department of Physics, Yale University, New Haven, CT, 06250-8121
[8] Physikalisches Institut, Universität Bonn, Nußallee 12, 53115 Bonn, Germany
[9] Department of Physics, University of California Berkeley, 366 LeConte Hall MC 7300, Berkeley, CA, 94720-7300
[10] Université de Lyon, F-69622, Lyon, France ; Université de Lyon 1, Villeurbanne ; CNRS/IN2P3, Institut de Physique Nucléaire de Lyon.
[11] Computational Cosmology Center, Computational Research Division, Lawrence Berkeley National Laboratory, 1 Cyclotron Road MS 50B-4206, Berkeley, CA, 94611
[12] Centre de Recherche Astronomique de Lyon, Université Lyon 1, 9 Avenue Charles André, 69561 Saint Genis Laval Cedex, France
[13] Centre de Physique des Particules de Marseille , 163, avenue de Luminy - Case 902 - 13288 Marseille Cedex 09, France
[14] Tsinghua Center for Astrophysics, Tsinghua University, Beijing 100084, China
[15] National Astronomical Observatories, Chinese Academy of Sciences, Beijing 100012, China

Hayden et al. 2010). Assuming a distance to M101 of 6.4 Mpc (Shappee & Stanek 2011), SN 2011fe is a normal SN Ia with $M_{B,\max} = -19.13$, having produced $\sim 0.6\,M_\odot$ of ^{56}Ni (Stritzinger et al. 2006). The identification of SN 2011fe as a prototypical SN Ia is also corroborated by the observed spectra (as shown below).

With the development of three-dimensional simulations of thermonuclear explosions in carbon–oxygen WDs and of the subsequent radiative transfer (RT) leading to the formation of the observables, a new generation of models is currently becoming available. These have the advantage that the explosion physics is represented in a far less parameterized manner than in previous one-dimensional models. Due to their improved predictive power, a comparison with observational data would in principle allow us to constrain the explosion scenario of SNe Ia. However, no currently available multi-dimensional model reaches the level of agreement that can be obtained fitting one-dimensional semi-empirical models to data. This challenges the interpretation of the comparison between the new models and SN Ia data.

Here, we address the question of whether SN 2011fe can be explained by models of an exploding Chandrasekhar-mass WD (realized as a delayed detonation) or a violent merger of two WDs. These scenarios can lead to observables that resemble normal SNe Ia (Mazzali et al. 2007; Kasen et al. 2009; Pakmor et al. 2012), but they differ fundamentally in the explosion mechanism, the mass and the structure of the ejecta. A discrimination between them based on comparison with observations would help to shed light on the open question of the progenitor system. An explosion of the WD near the Chandrasekhar mass is usually attributed to the single-degenerate progenitor channel in which a carbon-oxygen WD accretes matter from a non-degenerate companion; however, the formation of a Chandrasekhar-mass object in a merger of two WDs cannot be excluded. Our second scenario results from the merger of two WDs with similar and rather high masses adding up to a total of $2\,M_\odot$. Both models are set up to produce $\sim 0.6\,M_\odot$ of ^{56}Ni but apart from that they follow generic assumptions and are not tuned to fit the data of SN 2011fe.

2. EXPLOSION MODELS

The most promising way of producing observables in reasonable agreement with observations of normal SNe Ia from an explosion of a Chandrasekhar-mass WD is the delayed detonation mechanism (Khokhlov 1991). We model this scenario using the techniques described by Reinecke et al. (1999); Röpke & Hillebrandt (2005); Schmidt et al. (2006) and Röpke & Niemeyer (2007).

An isothermal ($T = 5 \times 10^5$ K) WD composed of carbon and oxygen in equal parts by mass was set up in hydrostatic equilibrium with a central density of $2.9 \times 10^9\,\mathrm{g\,cm^{-3}}$ and an electron fraction of $Y_e = 0.498864$, corresponding to solar metallicity. The model was discretized on a three-dimensional Cartesian moving grid (Röpke 2005) with 512^3 cells consisting of two nested parts. To reach the intended ^{56}Ni production, the initial deflagration was ignited in 100 sparks placed randomly in a Gaussian distribution within a radius of 150 km from the WD's center on the inner grid, which had a resolution of 1.92×10^5 cm. After an initial deflagration phase similar to that described by Röpke et al. (2007), a detonation was triggered at every location on the flame where the fuel density was in the range of 6 to $7 \times 10^6\,\mathrm{g\,cm^{-3}}$ and the grid cell contained preferentially fuel material, provided that the turbulent velocity fluctuations exceeded $10^8\,\mathrm{cm\,s^{-1}}$ at a significant fraction of the flame area and persisted for sufficiently long times. This loosely follows the criteria proposed by Woosley et al. (2009). Since the initiation of a detonation proceeds on scales that are not resolved in our simulations, the probability of finding high turbulent velocities on unresolved scales is extrapolated applying the procedure of Röpke (2007). The evolution was followed to a time of 100 s after ignition, by which homologous expansion of the ejecta was reached to a good approximation. This model, called N100, is part of a larger set of delayed-detonation simulations (Seitenzahl et al., in preparation).

The details of the nucleosynthesis in this explosion were determined from thermodynamic trajectories recorded by 10^6 tracer particles distributed in the exploding WD (Travaglio et al. 2004; Seitenzahl et al. 2010). The characteristics of the model are summarized in Table 1.

The second simulation we discuss models the inspiral, merger and explosion of two WDs with $1.1\,M_\odot$ and $0.9\,M_\odot$, respectively. Details of the corresponding simulations are given by Pakmor et al. (2012). While the inspiral and merger phases were followed with a version of the SPH code Gadget (Springel 2005), the subsequent thermonuclear detonation was modeled with techniques similar to those employed in N100. The question of whether a detonation triggers at the interface between the two merging stars is controversial. Simulations with sufficiently high numbers of SPH particles, such as presented here, show the formation of a hot spot, and we assume a detonation to trigger at this location when the temperature exceeds 2.5×10^9 K in material of $\rho \approx 2 \times 10^6\,\mathrm{g\,cm^{-3}}$, relying on the microscopic simulations of detonation initiation by Seitenzahl et al. (2009a). Again, the evolution was followed up to 100 s and the composition of the ejecta was determined in a post-processing step. The results of this simulation are given in Table 1.

Density and composition of both models in homologous expansion are visualized in Figs. 1 and 2. We note that the ejecta structure resulting from the WD-WD merger differs fundamentally from that of N100. This is because the explosion of the secondary WD happens shortly after that of the primary. Therefore, the outer ejecta material originates from the primary. At the onset of the explosion, the primary had a radius below $0.02\,R_\odot$ making our *violent* merger scenario consistent with the constraint on the radius of the exploding object derived by Bloom et al. (2012).

3. COMPARISON WITH SPECTRA OF SN 2011fe

From the nucleosynthesis tracer particles we constructed detailed abundance distributions of the explosion ejecta at 100 s and mapped them to 50^3 Cartesian grids. These grids were then used to derive synthetic light curves and spectra with the Monte Carlo RT code Artis (Kromer & Sim 2009; Sim 2007). To this end, we simulated the propagation of 10^8 photon packets from 2 to 120 days after explosion using the cd23_gf-5 atomic dataset of Kromer & Sim (2009), which

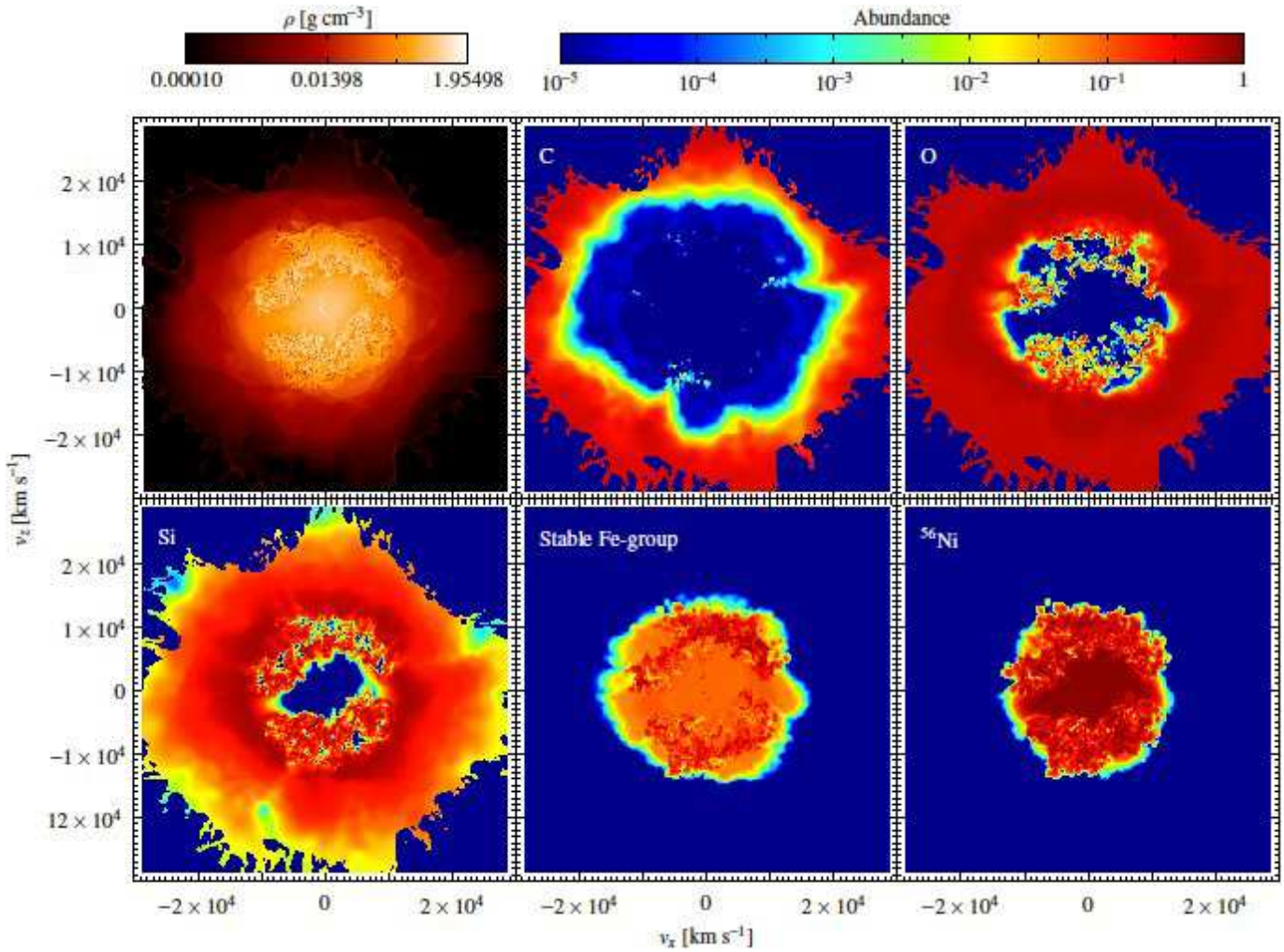

Figure 1. Slices through our delayed-detonation model N100 in the x–z-plane showing the density (top left) and abundance distribution of selected species at 100 s after explosion.

Table 1
Model characteristics.

	delayed detonation (N100)	violent merger
total ejecta mass [$M_\odot$]	1.40	1.95[a]
asymptotic kinetic energy of ejecta [10^{51} erg]	1.45	1.7
^{56}Ni mass [$M_\odot$]	0.604	0.616
total iron group [$M_\odot$]	0.839	0.697
total intermediate mass elements [$M_\odot$]	0.454	0.5
carbon mass [$M_\odot$]	0.003	0.153
oxygen mass [$M_\odot$]	0.101	0.492
combined mass of ^{55}Fe and ^{55}Co [$M_\odot$]	1.33×10^{-2}	3.73×10^{-3}
combined mass of ^{57}Ni and ^{57}Co [$M_\odot$]	1.88×10^{-2}	1.49×10^{-2}
B-band rise time [days]	16.6	20.8
B-band peak luminosity [mag]	−19.0	−19.0
$\Delta m_{15}(B)$ [mag]	1.34	0.95
$\mathrm{D}^{500}_{\mathrm{late}} \equiv m_{1400\mathrm{d}} - m_{900\mathrm{d}}$ in leptonic light curve [mag]	2.25	2.65
$\mathrm{D}^{1000}_{\mathrm{late}} \equiv m_{1900\mathrm{d}} - m_{900\mathrm{d}}$ in leptonic light curve [mag]	3.20	3.87

[a] 0.05 $\mathrm{M}_\odot$ are lost during the explosion simulation because of the finite extent of the grid

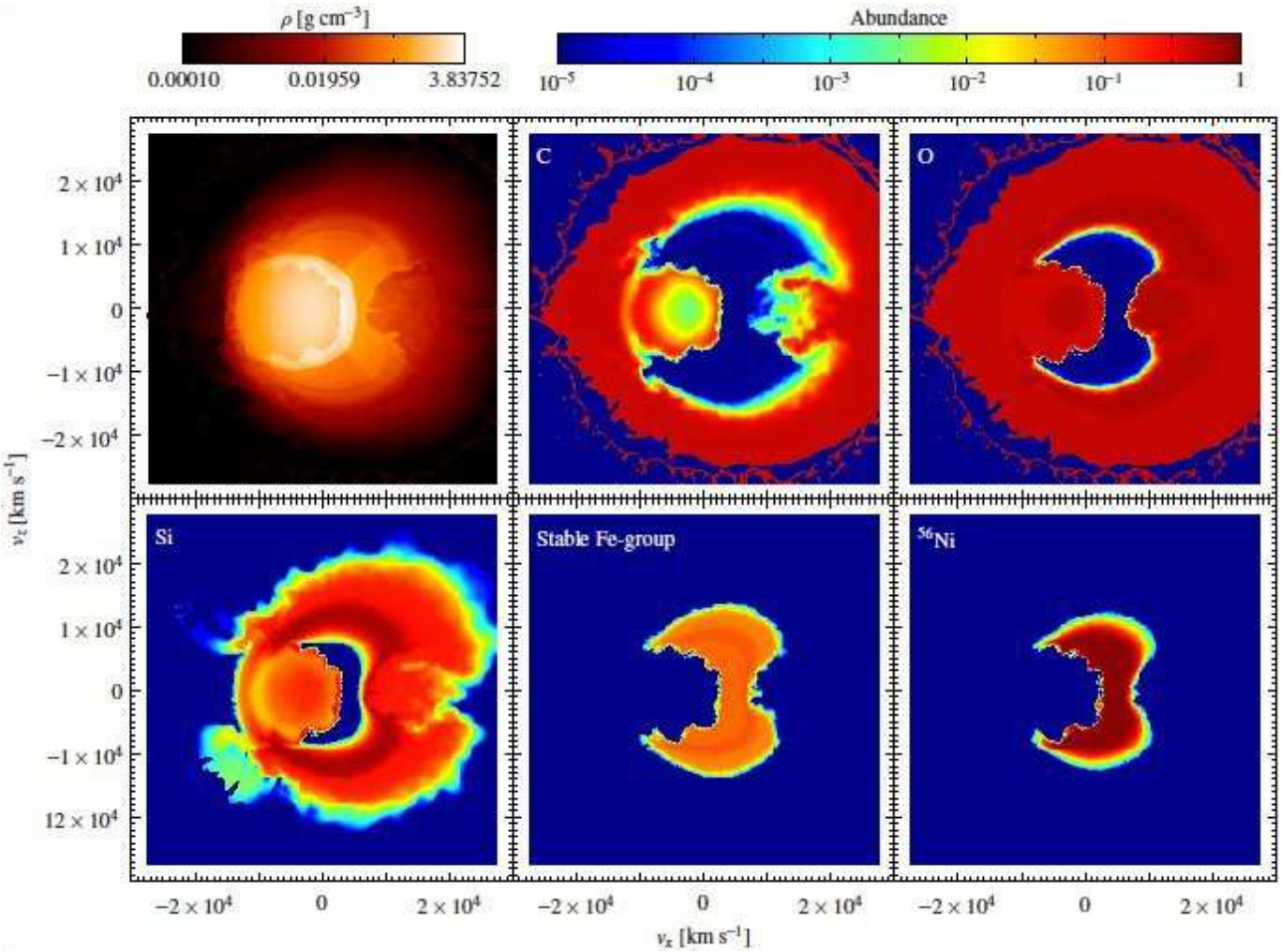

Figure 2. Same as Fig. 1 but for the merger model.

is based on the lines contained in the CD23 compilation of Kurucz & Bell (1995). To account for higher ionization at early times, we added the ionization stages VI and VII for Sc to Ni, leading to a total of $\sim 5 \times 10^5$ atomic lines.

Both our models yield a B-band peak magnitude of -19.0, roughly in agreement with that observed for SN 2011fe. Their rise times, however, differ: while N100 reaches B-band maximum after 16.6 d, the merger takes 20.8 d (further parameters of our synthetic light curves are given in Table 1). Thus, neither of the models gives a perfect match to the light curves of SN 2011fe but both are sufficiently close to warrant further investigation.

In Fig. 3 we compare synthetic spectra from our models with flux-calibrated spectra of SN 2011fe taken by the SNfactory collaboration with the SNIFS instrument (Aldering et al. 2002) on the University of Hawaii 2.2 m telescope on Mauna Kea. To our knowledge this is the first direct comparison of consistent three-dimensional SN Ia models with a spectrophotometric time-series. Overall, the spectra of both explosion scenarios reproduce the main features of the observed spectra and the flux level reasonably well (note that these are not fits but predictions from "first-principle" models and that *absolute* fluxes are compared). In detail, however, there are problems in both models.

The predicted absorption features are blue-shifted with respect to the observations. Although this effect is stronger in N100, it is also visible for the merger, indicating too high ejecta velocities in the models. Since the mass of the exploding object is very different in the two cases, the nuclear energy release is likely too high in both explosion processes. A potential way to cure this problem is to increase the oxygen abundance in the progenitor WDs at the expense of carbon thus increasing the average nuclear binding energy of the fuel.

While N100 is only marginally too bright at the early epochs, the merger is clearly too faint. This corresponds to the shorter/longer rise time of the respective model (see Tab. 1) compared to SN 2011fe. Around B-band maximum at $\sim$18 d the merger compares favorably to the observed spectra. The flux level and the overall shape of its synthetic spectra match the data better than those of N100. After maximum the agreement with the observations deteriorates for both models, although the effect is more drastic for N100. In particular, the models fail to reproduce the spectral features between 5000 Å and 6000 Å. Moreover, both models become redder faster than the observation. Again, this trend is more pronounced in N100, but is also visible in the merger.

Figs. 1 and 2 show that iron-group elements (IGEs) extend significantly beyond velocities of $10,000\,\mathrm{km\,s^{-1}}$ in N100 but also in some directions in the merger. The W7 model of Nomoto et al. (1984), which is known to reproduce observables of SNe Ia well, does not contain IGEs at such high velocities. However, they are reported in abundance tomographies of the normal SNe 2002bo (Stehle et al. 2005) and 2004eo (Mazzali et al. 2008) and Nugent et al. (2011b) identify iron in the earliest spectra of SN 2011fe at velocities of $16,000\,\mathrm{km\,s^{-1}}$. Our synthetic spectra do not show mismatches with observed lines that can be directly attributed to high-velocity IGEs. It is possible, however, that they contribute to the fast reddening of the models. As for the high ejecta velocities, a decreased carbon/oxygen ratio in the exploding WDs may alleviate this problem.

An important difference between the two models is also visible from Figs. 1 and 2: N100 is—apart from small-scale anisotropies—roughly spherical (see also Blondin et al. 2011). In contrast, the merger shows pronounced large-scale asymmetries. This is reflected in a strong viewing-angle dependence in its spectra which increases after maximum due to the growing asymmetry of the inner ejecta for smaller radii. As demonstrated in the lower plot of Fig. 3 individual line-of-sight spectra from the merger reproduce the observation at least as well as the angle-average. Nevertheless, the high level of asymmetry in the merger could be in conflict with the observed spectral homogeneity of normal SNe Ia and the low level of continuum polarization observed (Wang & Wheeler 2008). Currently our RT simulations do not include polarization. Note, however, that Smith et al. (2011) report a continuum polarization of 0.2–0.4% for SN 2011fe which they interpret as a sign of persistent asymmetry in the last-scattering surface.

The fact that the merger reproduces the observed spectra better than N100 at maximum light (and later) suggests that the chemical structure of its deeper ejecta, which dominate the spectrum formation at this epoch, is closer to that of SN 2011fe. Since neither of the models matches the optical data of early epochs perfectly, our comparison gives slight preference to a WD merger scenario over a delayed detonation in a Chandrasekhar-mass WD as an explanation for this object. But as there are major shortcomings in both models, a definitive conclusion cannot be drawn. Observables other than maximum-light spectra may, however, have more discriminating power. We discuss promising possibilities in the following.

4. LATE-TIME OBSERVABLES

While optical data taken before and around peak brightness probe predominantly the outermost layers, observations at later epochs are sensitive to the core of the ejecta. Since this is the region where the differences between the two models considered here are most pronounced, late-time observables are a very useful diagnostic tool.

A fundamental difference between our two explosion scenarios is the density at which the material is burned in the thermonuclear combustion. Due to the high central density of the Chandrasekhar-mass WD, substantial burning proceeds on thermodynamic trajectories with peak densities above $2\times10^8\,\mathrm{g\,cm^{-3}}$ in N100 (especially in its deflagration phase), whereas in the violent merger all the burning occurs at peak densities below $2\times10^8\,\mathrm{g\,cm^{-3}}$. This leads to vastly different degrees of neutronization in the ashes due to electron capture reactions, resulting in higher abundances of stable IGEs (in particular ^{54}Fe, ^{56}Fe, and ^{58}Ni) for N100 which should be reflected in the presence of Ni lines in spectra from the nebular phase (Maeda et al. 2010b; Gerardy et al. 2007). Moreover, our models differ significantly in composition and geometry of the innermost ejecta. While the ^{56}Ni distribution is roughly spherical for N100, most of the ^{56}Ni is off-center in the merger. Asymmetric and shifted lines can be expected here and could correspond to the effects

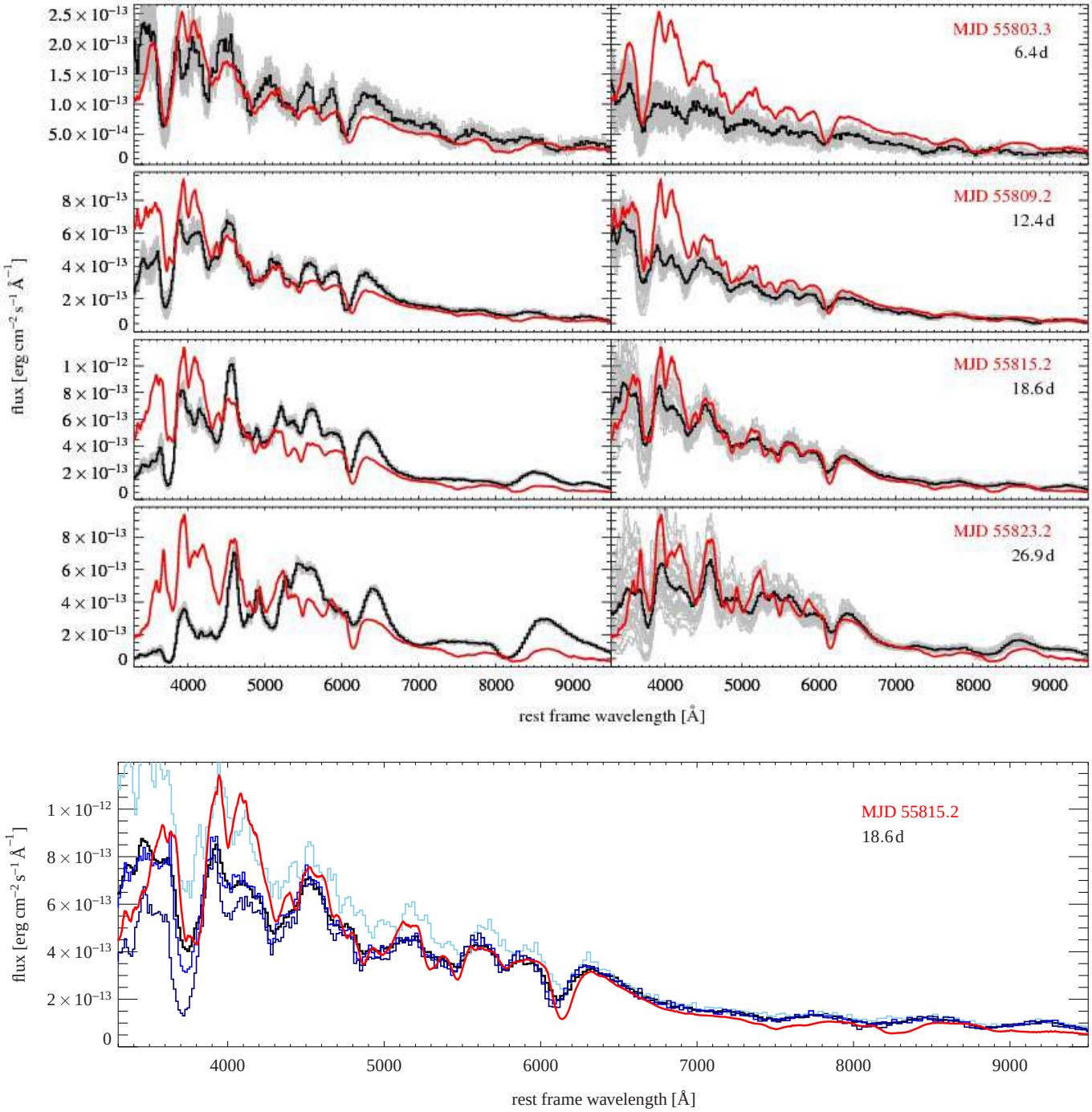

Figure 3. Spectral evolution of our delayed detonation N100 (left) and merger model (right) from 6 to 27 days after the explosion. The angle-averaged spectrum is plotted in black while 25 spectra for representative viewing angles are shown in gray (the variability with viewing angle of the earliest spectra is dominated by Monte Carlo noise in both models). For comparison the observed spectra of SN 2011fe are over-plotted in red assuming an explosion date at August 23.7 (MJD 55796.7; Nugent et al. 2011b). The observations were corrected for Galactic reddening assuming $E(B-V)_{\rm Gal} = 0.009\,{\rm mag}$ (Schlegel et al. 1998) and de-redshifted according to a heliocentric radial velocity $v_{\rm hel} = 241\,{\rm km\,s^{-1}}$ given by de Vaucouleurs et al. (1991). Reddening from the host is negligible. The bottom panel compares the observed spectrum of SN 2011fe near B-band maximum (red) with synthetic spectra from the merger corresponding to three different viewing angles (blue colors) and the angle-average (black).

discussed by Maeda et al. (2010b,a). In the merger, the detonation of the secondary WD at low densities produces copious amounts of oxygen in the innermost ejecta. Potentially, this could lead to strong [OI] $\lambda\lambda$6300,6364 emission at late times (Kozma et al. 2005), which is not observed in SNe Ia. The efficiency of [OI] emission, however, depends strongly on the contamination with other elements and the ionization state of the oxygen-rich zone. For strong ionization (as might be the case in our low-density core), the presence of oxygen in the core would pose no problem for the merger. Clearly, nebular spectra contain important information, but a firm conclusion can only be drawn upon detailed three-dimensional modeling of the late-time RT, which is beyond the scope of this letter.

There is, however, a more direct and perhaps more easily studied effect. Due to the low central densities of the two sub-Chandrasekhar mass WDs, all of the IGEs in the merger are synthesized in either α-rich freeze-out from nuclear statistical equilibrium or in incomplete Si-burning. In contrast, much of it is produced under "normal" freeze-out conditions in the deflagration phase of N100 (Thielemann et al. 1986 place the dividing line between α-rich and "normal" freeze-out at $\sim 2\times10^8\,\mathrm{g\,cm^{-3}}$ for explosive burning of C+O material in SNe Ia). This leads to a higher abundance of ^{55}Co—an isotope mainly synthesized in the "normal" freeze-out and in incomplete Si-burning (e.g. Thielemann et al. 1986)—in the ejecta of the Chandrasekhar-mass WD explosion than in those of the merger.

Such different isotopic ratios in the IGEs affect the shapes of the predicted late-time light curves (Seitenzahl et al. 2009b). Starting at $\sim$800 d after the explosion, the *leptonic light curves* that assume full transparency to γ-rays and pure leptonic heating of the ejecta will be increasingly powered by the decay of isotopes other than ^{56}Co. This is illustrated in Fig. 4. At $\sim$1000 d after the explosion, the decay of ^{57}Co to ^{57}Fe, which (in $\sim$80% of all decays) emits internal conversion electrons, starts to dominate the light curves. Later, the decay of ^{55}Fe, which is mainly synthesized as ^{55}Co, to ^{55}Mn (a ground-state to ground-state transition followed by the emission of Auger electrons) contributes significantly and eventually dominates the radioactive energy generation.

The leptonic light curve of N100 will fall off more slowly than that of the merger. For example, the decrease in combined leptonic energy production from 900 d to 1400 d (1900 d) corresponds to a dimming by 2.25 (3.20) magnitudes for N100 and by 2.65 (3.87) magnitudes for the merger (see Table 1).

Thus, a measurement of the late light curve decline rate would distinguish between an explosion of a Chandrasekhar-mass WD (which in any scenario requires some pre-expansion in a deflagration stage) and alternative models based on detonations in low density material—such as mergers of WDs. For this, neither the correct distance to the object nor the exact ^{56}Ni production have to be known. Note, however, that the light curves shown are idealized cases assuming that the leptonic energy production rates can be directly translated into UVOIR light curves (which may be precluded by effects such as the infrared catastrophe, "frozen-in ionization", CSM interaction, leptonic losses, etc.).

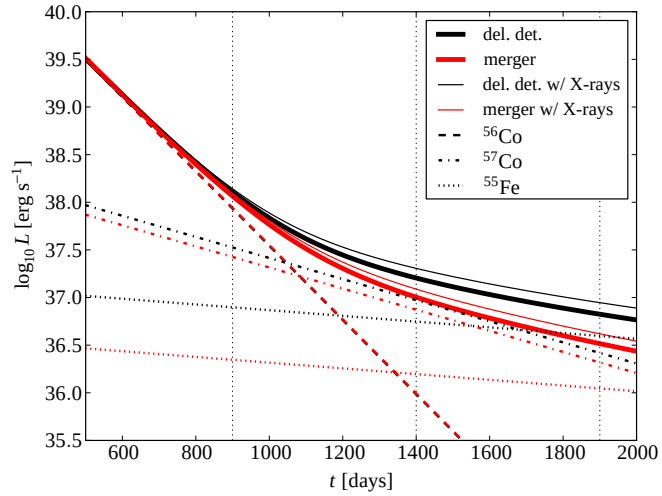

Figure 4. Leptonic luminosity as a function of time after the explosion for N100 (black bold line) and the merger model (red bold line). The dashed, dash-dotted and dotted lines give the contribution to the leptonic luminosity due to the decay of selected isotopes. Thin solid lines give the luminosities including decay X-rays.

5. CONCLUSIONS

Although the nearby SN 2011fe offers a unique opportunity to scrutinize explosion models, at present a clear preference of one scenario over the other is hard to establish. We therefore discuss two models that are very distinct in the explosion characteristics and in the resulting structure of the ejecta—a delayed detonation of a Chandrasekhar-mass WD and a merger of two WDs with a total of $2\,M_\odot$.

Comparing with early and near-maximum optical spectra, both scenarios reproduce the main features but the merger is slightly preferred because it provides a better match to the observations around peak brightness. There are, however, shortcomings in other aspects—such as the too long rise time—and therefore the working hypothesis of SN 2011fe resulting from a merger of two WDs requires additional confirmation.

As shown here, alternatives to early-phase optical data may have more decisive power. At very late epochs nucleosynthetic effects lead to different characteristics in the photometric evolution that may allow us to discriminate between explosion models. This, however, requires true bolometric measurements, and it is unclear at which wavelengths the maximum emission occurs at those late epochs. Observations of SN 2011fe will help to clarify this issue and thus multi-wavelength monitoring of this object is essential. If the maximum emission falls into the optical range, a clear distinction between explosion models (that can then be related to progenitor scenarios) will be possible from photometric measurements at $\gtrsim$1000 d. Thanks to its proximity, these observations should be feasible for SN 2011fe.

This work was supported by the Deutsche Forschungsgemeinschaft via the Transregional Collaborative Research Center TRR 33, the Emmy Noether Program (RO 3676/1-1) and the Excellence Cluster EXC 153, DOE Contracts DE-AC02-05CH1123 and DE-AC02-05CH11231, the Gordon & Betty Moore Foundation, CNRS/IN2P3, CNRS/INSU, and PNC in France, the Max Planck Society, and the Tsinghua University Cen-

ter for Astrophysics. The simulations were performed at JSC (grants PRACE042 and HMU014) and NCI at the ANU. We are grateful to C. Aspin, E. Gaidos, A. Mann, M. Micheli, T. Riesen, S. Sonnett, and D. Tholen, who granted us interrupt time to observe SN 2011fe.

REFERENCES

Aldering, G., Adam, G., Antilogus, P., Astier, P., Bacon, R., Bongard, S., Bonnaud, C., Copin, Y., Hardin, D., Henault, F., Howell, D. A., Lemonnier, J.-P., Levy, J.-M., Loken, S. C., Nugent, P. E., Pain, R., Pecontal, A., Pecontal, E., Perlmutter, S., Quimby, R. M., Schahmaneche, K., Smadja, G., & Wood-Vasey, W. M. 2002, in Society of Photo-Optical Instrumentation Engineers (SPIE) Conference Series, Vol. 4836, Survey and Other Telescope Technologies and Discoveries., ed. J. A. Tyson & S. Wolff, 61–72

Blondin, S., Kasen, D., Röpke, F. K., Kirshner, R. P., & Mandel, K. S. 2011, MNRAS, 417, 1280

Bloom, J. S., Kasen, D., Shen, K. J., Nugent, P. E., Butler, N. R., Graham, M. L., Howell, D. A., Kolb, U., Holmes, S., Haswell, C. A., Burwitz, V., Rodriguez, J., & Sullivan, M. 2012, ApJ, 744, L17

Brown, P. J., Dawson, K. S., de Pasquale, M., Gronwall, C., Holland, S., Immler, S., Kuin, P., Mazzali, P., Milne, P., Oates, S., & Siegel, M. 2011, ArXiv e-prints

Conley, A., Howell, D. A., Howes, A., Sullivan, M., Astier, P., Balam, D., Basa, S., Carlberg, R. G., Fouchez, D., Guy, J., Hook, I., Neill, J. D., Pain, R., Perrett, K., Pritchet, C. J., Regnault, N., Rich, J., Taillet, R., Aubourg, E., Bronder, J., Ellis, R. S., Fabbro, S., Filiol, M., Le Borgne, D., Palanque-Delabrouille, N., Perlmutter, S., & Ripoche, P. 2006, AJ, 132, 1707

de Vaucouleurs, G., de Vaucouleurs, A., Corwin, Jr., H. G., Buta, R. J., Paturel, G., & Fouqué, P. 1991, Third Reference Catalogue of Bright Galaxies (Berlin Heidelberg New York: Springer-Verlag)

Gerardy, C. L., Meikle, W. P. S., Kotak, R., Höflich, P., Farrah, D., Filippenko, A. V., Foley, R. J., Lundqvist, P., Mattila, S., Pozzo, M., Sollerman, J., Van Dyk, S. D., & Wheeler, J. C. 2007, ApJ, 661, 995

Hayden, B. T., Garnavich, P. M., Kessler, R., Frieman, J. A., Jha, S. W., Bassett, B., Cinabro, D., Dilday, B., Kasen, D., Marriner, J., Nichol, R. C., Riess, A. G., Sako, M., Schneider, D. P., Smith, M., & Sollerman, J. 2010, ApJ, 712, 350

Kasen, D., Röpke, F. K., & Woosley, S. E. 2009, Nature, 460, 869

Khokhlov, A. M. 1991, A&A, 245, 114

Kozma, C., Fransson, C., Hillebrandt, W., Travaglio, C., Sollerman, J., Reinecke, M., Röpke, F. K., & Spyromilio, J. 2005, A&A, 437, 983

Kromer, M., & Sim, S. A. 2009, MNRAS, 398, 1809

Kurucz, R., & Bell, B. 1995, Cambridge, Mass.: Smithsonian Astrophysical Observatory.

Li, W., Bloom, J. S., Podsiadlowski, P., Miller, A. A., Cenko, S. B., Jha, S. W., Sullivan, M., Howell, D. A., Nugent, P. E., Butler, N. R., Ofek, E. O., Kasliwal, M. M., Richards, J. W., Stockton, A., Shih, H.-Y., Bildsten, L., Shara, M. M., Bibby, J., Filippenko, A. V., Ganeshalingam, M., Silverman, J. M., Kulkarni, S. R., Law, N. M., Poznanski, D., Quimby, R. M., McCully, C., Patel, B., Maguire, K., & Shen, K. J. 2011, Nature, 480, 348

Liu, J., Di Stefano, R., Wang, T., & Moe, M. 2011, ArXiv e-prints

Maeda, K., Benetti, S., Stritzinger, M., Röpke, F. K., Folatelli, G., Sollerman, J., Taubenberger, S., Nomoto, K., Leloudas, G., Hamuy, M., Tanaka, M., Mazzali, P. A., & Elias-Rosa, N. 2010a, Nature, 466, 82

Maeda, K., Taubenberger, S., Sollerman, J., Mazzali, P. A., Leloudas, G., Nomoto, K., & Motohara, K. 2010b, ApJ, 708, 1703

Mazzali, P. A., Röpke, F. K., Benetti, S., & Hillebrandt, W. 2007, Science, 315, 825

Mazzali, P. A., Sauer, D. N., Pastorello, A., Benetti, S., & Hillebrandt, W. 2008, MNRAS, 386, 1897

Nomoto, K., Thielemann, F.-K., & Yokoi, K. 1984, ApJ, 286, 644

Nugent, P., Sullivan, M., Bersier, D., Howell, D. A., Thomas, R., & James, P. 2011a, The Astronomer's Telegram, 3581, 1

Nugent, P. E., Sullivan, M., Cenko, S. B., Thomas, R. C., Kasen, D., Howell, D. A., Bersier, D., Bloom, J. S., Kulkarni, S. R., Kandrashoff, M. T., Filippenko, A. V., Silverman, J. M., Marcy, G. W., Howard, A. W., Isaacson, H. T., Maguire, K., Suzuki, N., Tarlton, J. E., Pan, Y.-C., Bildsten, L., Fulton, B. J., Parrent, J. T., Sand, D., Podsiadlowski, P., Bianco, F. B., Dilday, B., Graham, M. L., Lyman, J., James, P., Kasliwal, M. M., Law, N. M., Quimby, R. M., Hook, I. M., Walker, E. S., Mazzali, P., Pian, E., Ofek, E. O., Gal-Yam, A., & Poznanski, D. 2011b, Nature, 480, 344

Pakmor, R., Kromer, M., Taubenberger, S., Sim, S. A., Röpke, F. K., & Hillebrandt, W. 2012, ApJ, 747, L10

Reinecke, M., Hillebrandt, W., Niemeyer, J. C., Klein, R., & Gröbl, A. 1999, A&A, 347, 724

Röpke, F. K. 2005, A&A, 432, 969

—. 2007, ApJ, 668, 1103

Röpke, F. K., & Hillebrandt, W. 2005, A&A, 431, 635

Röpke, F. K., Hillebrandt, W., Schmidt, W., Niemeyer, J. C., Blinnikov, S. I., & Mazzali, P. A. 2007, ApJ, 668, 1132

Röpke, F. K., & Niemeyer, J. C. 2007, A&A, 464, 683

Schlegel, D. J., Finkbeiner, D. P., & Davis, M. 1998, ApJ, 500, 525

Schmidt, W., Niemeyer, J. C., Hillebrandt, W., & Röpke, F. K. 2006, A&A, 450, 283

Seitenzahl, I. R., Meakin, C. A., Townsley, D. M., Lamb, D. Q., & Truran, J. W. 2009a, ApJ, 696, 515

Seitenzahl, I. R., Röpke, F. K., Fink, M., & Pakmor, R. 2010, MNRAS, 407, 2297

Seitenzahl, I. R., Taubenberger, S., & Sim, S. A. 2009b, MNRAS, 400, 531

Shappee, B. J., & Stanek, K. Z. 2011, ApJ, 733, 124

Sim, S. A. 2007, MNRAS, 375, 154

Smith, P. S., Williams, G. G., Smith, N., Milne, P. A., Jannuzi, B. T., & Green, E. M. 2011, ArXiv e-prints

Springel, V. 2005, MNRAS, 364, 1105

Stehle, M., Mazzali, P. A., Benetti, S., & Hillebrandt, W. 2005, MNRAS, 360, 1231

Stritzinger, M., Leibundgut, B., Walch, S., & Contardo, G. 2006, A&A, 450, 241

Thielemann, F.-K., Nomoto, K., & Yokoi, K. 1986, A&A, 158, 17

Travaglio, C., Hillebrandt, W., Reinecke, M., & Thielemann, F.-K. 2004, A&A, 425, 1029

Wang, L., & Wheeler, J. C. 2008, ARA&A, 46, 433

Woosley, S. E., Kerstein, A. R., Sankaran, V., Aspden, A. J., & Röpke, F. K. 2009, ApJ, 704, 255